

Development of Fatigue Damages in a Pseudo- α -Titanium Alloy after Intense Thermomechanical Treatment

V. P. Bagmutov^{a, *}, V. I. Vodop'yanov^a, I. N. Zakharov^a, A. V. Vdovenko^a,
M. D. Romanenko^a, and V. V. Chekunov^a

^aVolgograd State Technical University, Volgograd, 400006 Russia

*e-mail: sopromat@vstu.ru

Received December 8, 2017; revised February 28, 2018; accepted March 28, 2018

Abstract—The influence of surface hardening by electrochemical treatment, abrasive-free ultrasonic finishing treatment, and their combination on the accumulation of fatigue damages in a pseudo- α -titanium alloy (PT3V) during pulsed cyclic loading in a transition stage of fatigue (10^4 – 10^5 cycles) is studied. The fatigue damage accumulation kinetics is estimated using the inelasticity parameters of a specimen (hysteresis loop width, cyclic creep, rigidity (compliance)) during cyclic loading, an analysis of fracture surfaces, and the crack growth rate. The state of surface layer is shown to play a key role in the change in the fatigue life of laboratory specimens. The type of surface hardening only weakly affects the accumulation of fatigue damages at the stages of stable crack growth and rupture.

Keywords: titanium alloy, surface hardening, electromechanical treatment, ultrasonic treatment, fatigue life, fractography, inelasticity, fatigue crack growth

DOI: 10.1134/S0036029519050033

INTRODUCTION

Fatigue strength and fatigue life are important criteria for estimating the functionality and the resource of parts and structures intended for various purposes. Their role becomes very important in modern highly loaded and important parts, which undergo cyclic loads in both high- and low-cycle fatigue ranges. Therefore, it is important to understand a damage accumulation mechanism and to control a structure to form wear-resistant and high-fatigue-strength surface layers in parts, in particular, those made of titanium alloys.

The importance of these points increases due to the development and implementation of various methods of modifying the surface layers in structural materials, including high-energy actions, to increase their wear resistance and fatigue strength [1, 2].

The main factors, a combination of which determines changes in the behavior of surface-hardened titanium alloy specimens during cyclic loading, are as follows:

(a) the microstructure of the surface layer of the base metal (globular, lamellar, bimodal, coarse-grained, fine-grained, ultrafine-grained structure and nanostructure) [3, 4];

(b) the level and distribution of residual stresses, which form in the surface layer of a material during surface treatment [5, 6];

(c) microgeometry parameters, the roughness of hardened surface, and the presence of regular structures [7, 8];

(d) the strength and plasticity characteristics and the geometric parameters of a hardened layer [4, 9].

Despite deep interest of researchers in the formation of the fatigue strength of titanium alloys during hardening by intense thermomechanical actions, the problems of fatigue crack nucleation and growth, the stage time, and the relation between these stages and the geometry and properties of hardened metal regions are still poorly understood. The influence of these factors can differently affect the mechanisms of accumulation of fatigue damage and fatigue fracture. In some cases, surface hardening treatment of titanium alloys, e.g., the treatment increasing their wear resistance, can be accompanied by both a decrease and an increase in the fatigue strength depending on the state of the surface layer and its parameters [9].

The accumulation of fatigue damages is known to include the stages of initial volume-distributed fatigue damage accumulation, crack nucleation, localized fatigue damage (which manifests itself in stable fatigue crack growth), and accelerated macrocrack growth to rupture [10, 11]. The laws of damage development at each stage are important to achieve reliable and long-term operation of a part and to develop reliable methods for calculating the cyclic strength [10]. However, the diversity of surface layer hardening mechanisms

Table 1. Chemical composition of a PT3V-type alloy, wt %

Ti	Al	V	Zr	Fe	Si	C	O ₂	N ₂	H ₂
93	4.6	1.9	0.2	0.015	0.12	0.006	0.1	0.03	0.006

under various actions, the wide spectrum of the stress cycle characteristics, and the complexity of experiments make it difficult to experimentally determine the damage parameters and to develop reliable methods for calculating the fatigue strength and the fatigue life [11, 12]. Therefore, to study the accumulation of fatigue damages in surface-hardened titanium alloys and to estimate their influence on the total fatigue life using the methods that are sensitive to the structural state of a structural material are challenging problems. Such investigations are related to a study of inelasticity effects (cyclic creep, hysteresis loop width, compliance of a specimen), an analysis of microfractographic fracture surfaces, and an investigation of the laws of fatigue crack growth using classical approaches such as the Paris model.

In [13], we studied the influence of the parameters of thermomechanical hardening treatment on the hardness and the microstructure of a pseudo- α -titanium 5V alloy and found the most effective hardening version. In [14], we investigated changes in the microhardness and the fatigue life of a pseudo- α -titanium alloy and described the mechanisms of fracture and the structures of crack nucleation and growth regions during combined hardening treatment.

This work is a continuation of the studies performed in [13, 14]. The purpose of this work is to analyze the influence of the state of the surface layer formed upon intense thermomechanical treatment at the stage of fatigue damages (crack nucleation and growth, rupture of specimens) by the investigation of changes in the inelastic properties, the fractography of the fracture surfaces of a pseudo- α -titanium alloy, and the fatigue crack growth in alloy specimens.

EXPERIMENTAL

We studied corset specimens made of a PT3V pseudo- α -titanium alloy (certified chemical composition of the alloy is given in Table 1) in an initial state after hot rolling and after surface hardening by the following three techniques: electromechanical treatment (EMT), surface abrasive-free ultrasonic finishing treatment (AUFT), and combined EMT and AUFT (EMT + AUFT).

Workpieces for the corset specimens were cut from a sheet along the rolling direction [14]. The structure of the alloy in the initial state is lamellar and consists of the transformed β phase with a coarse-lamellar α fraction (Fig. 1, region 1).

The mechanical properties of the alloy in the initial state were determined on cylindrical specimens of type

1Y (GOST 1497–84) 8 mm in diameter. The ultimate tensile strength was $\sigma_u = 875$ MPa, the yield strength was $\sigma_{0.2} = 770$ MPa, the relative elongation was $\delta = 9–11\%$, and the relative reduction of area was $\psi = 20–30\%$. The EMT and AUFT hardening processes were carried out on a standard turning lathe. A hardening process was adjusted by changing tool in a lathe toolholder. For EMT specimens, the conditions ensuring the maximum increase in the microhardness were as follows [13]: the current density was $j = 400$ A/mm², the treatment speed was $v = 0.61$ m/min, the feed speed was $S = 0.4$ mm/rev, the deforming force was $F = 500$ N, and the electrode tool consisted of conic rolls made of a VK6S hard alloy 60 mm in diameter with a sharpening angle of 5° and a contact band of 0.5–0.7 mm. The AUFT conditions were as follows: the emitter radiation frequency was 22 kHz, the treatment speed was $v = 4.71$ m/min, the feed speed was $S = 0.07$ mm/rev, and the deforming force was $F = 100$ N [13]. The conditions were also used for combined EMT + AUFT hardening.

Rapid heating and cooling of a titanium alloy during EMT are known to be accompanied by structure–phase transformations and hardening of the metal [13]. Figure 1 (region 2) shows the fine-grained

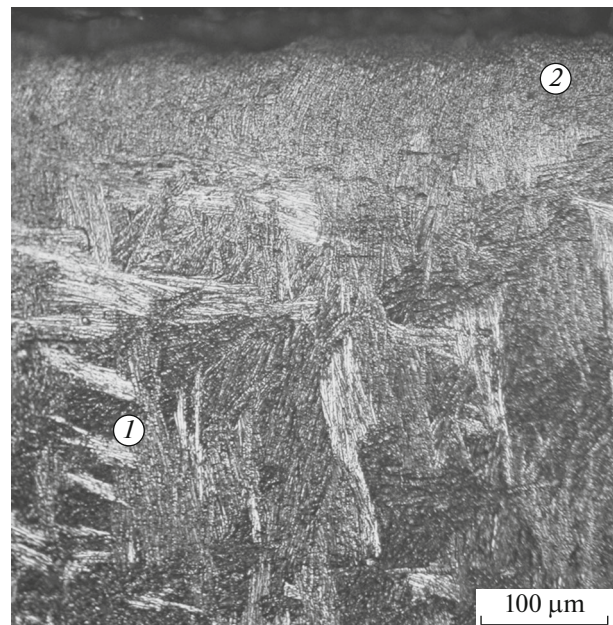


Fig. 1. Micrograph of a polished cross section of a PT3V titanium alloy at the boundary between the initial metal and the hardened surface layer: (1) initial structure of the alloy and (2) structure of the hardened layer.

Table 2. Effect of the state of specimen surface on the mechanical properties

Property	Surface treatment			
	initial	EMT	AUFT	EMT + AUFT
Microhardness, MPa	3800	5700	4370	5800
Relative change in microhardness	1	1.5	1.15	1.53
ultimate tensile strength	1	1.05	1.05	1.08
relative reduction of area	1	0.5	1.38	0.86
Number of cycles to failure $N_f \times 10^3$	87	19.1	98	111
Relative change in fatigue life	1	0.22	1.12	1.27

structure of the surface layer (0.1 mm deep) formed under these conditions.

The hardening of the surface layer was estimated from its microhardness. For this purpose, a series of 20 indentations at a load of 0.5 and 1 N on an indenter was made on the sample surface using a PMT-3M microhardness tester, and the indentation sizes were determined with the special-purpose VideoTest-Struktura software package.

Cyclic loading was carried out using corset specimens of type 1 (GOST 25.502–79) 8 mm in diameter on a servohydraulic BISS-100 kN testing machine interfaced with a PC. The loading frequency was 3 Hz. We used a zero-to-compression stress cycle with a stress ratio $R = 0.1$. During tests, we specified the maximum and minimum cycle loads, which were used to

calculate the maximum and minimum cycle stresses, respectively. In tests, we detected the maximum (e_{\max}) and minimum (e_{\min}) cycle strains and recorded mechanical hysteresis loops.

Metallographic analysis of the structures of the surface layer and the base metal after fatigue tests and a preliminary detection of a fracture zone were performed using a METAM LV-32 microscope. Fracture surfaces were studied by electron microscopy on a Versa 3D scanning electron microscope.

RESULTS AND DISCUSSION

Surface Microhardness and the Fatigue Life of Specimens

Influence of surface hardening on the mechanical properties of specimens. After specimen preparation and surface hardening, we measured the surface microhardness and performed cyclic loading to failure under the conditions described above. Table 2 gives the experimental results of measuring the microhardness, the strength and plasticity characteristics, and the fracture number of cycles N_f at $\sigma_{\max} = 0.8\sigma_{0.2}$. Figure 2 shows the segments of fatigue curves that correspond to the fatigue life for various types of surface treatment.

The surface hardening of a titanium alloy of type PT3V can be accompanied by a noticeable increase in the microhardness of the hardened layer: by 50% in the case of EMT and combined EMT + AUFT treatment (from 3800 MPa for initial specimens to 5700–5800 MPa after hardening) and by 15% in the case of AUFT (see Table 2).

The existence of a relatively thin hardened layer (depth of 1.25% of the diameter) on the specimen surface increases the ultimate tensile strength by 5% (after EMT and AUFT) or 8% (after EMT + AUFT). The relative reduction of area after EMT decreased twofold as compared to the initial state. AUFT increases the plasticity during static tension by 38% for specimens with the initial structure and by 72% for the EMT-hardened specimens (see Table 2).

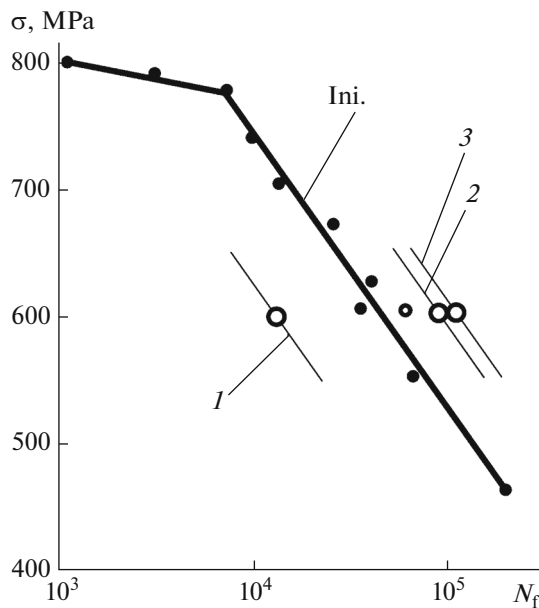


Fig. 2. Effect of surface hardening on the fatigue life of a pseudo- α -titanium alloy during tension (stress ratio of 0.1): (Ini.) initial state after polishing, (1) after EMT, (2) after AUFT, and (3) after EMT + AUFT.

An analysis of the fatigue curves of initial specimens revealed the following two stages for the alloy under study (see Fig. 2): quasi-static fracture and transition stage [10]. The stage of quasi-static fracture corresponds to a high level of stresses. As the stress amplitude decreases, the role of fatigue damages increases and the stage of quasi-static damage in the fatigue curve changes into the transition stage. The maximum stresses ($\sigma_{\max} = 0.8\sigma_{0.2}$) specified in experiments approximately correspond to the center of the stress range in the transition stage of the fatigue curve. For this stress level, we determined the fatigue lives of specimens with various states of the surface layer, namely, after polishing (initial state), EMT, AUFT, and EMT + AUFT (see Fig. 2).

As follows from these data, the presence of a hardened layer with a high microhardness on the specimen surface does not mean an analogous increase in the fatigue life: in some cases, the fatigue life even decreased (see Table 2). For example, the fatigue life of the PT3V alloy after EMT decreased by more than 75% (from 87000 cycles of the initial alloy to 19000 cycles for the EMT-hardened specimens), and AUFT leads to an increase in the fatigue life by 12% (98000 cycles) for the initial specimens and by 27% (111000 cycles) for the specimens after combined hardening EMT + AUFT.

The factor such as the embrittlement of the hardened surface metal, the formation of internal stress concentrators, and the formation of dangerous residual stresses during surface treatment are likely to be decisive in the cases of decreasing the fatigue lives of the specimens. The mathematical simulation of thermomechanical treatment during EMT of titanium alloys [15] demonstrates that tensile stresses appear in their surface layers, and the intense plastic deformation of a thin surface layer during AUFT is accompanied by the formation of compressive stresses. Along with the ultrafine-grained structure formed in the surface layer during treatment, these stresses can increase the fatigue life.

Change in the Inelasticity Characteristics

The development of fatigue damages in the loaded volume is accompanied by the accumulation of one-sided quasi-static deformation e and is expressed as a nonlinear stress–strain relation, which can be characterized by hysteresis loop width Δe (Fig. 3). Moreover, as a crack grows, the cross-sectional area and its rigidity decrease, which manifests itself in a decrease in the slope of the elastic loading line E_c (see Fig. 3) [11].

To determine the controlled parameters during cyclic tests, we recorded the loading and deformation parameters and mechanical hysteresis loops. Using these data, we determined the maximum (e_{\max}) and minimum (e_{\min}) cycle deformations and parameter E_c (see Fig. 3). The change in the minimum cycle defor-

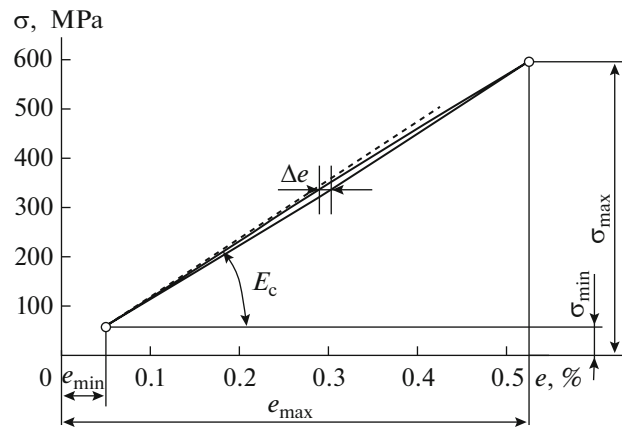


Fig. 3. Hysteresis loop in a loading–unloading cycle with specified (σ_{\max} , σ_{\min}) and controlled (E_c , e_{\min} , Δe) parameters.

mation e_{\min} during tests was taken to be cyclic creep deformation e , the change in the hysteresis loop width Δe was used to estimate the degree of fatigue damages, and E_c at the stage of crack growth reflected the compliance of a specimen.

Figure 4 shows the characteristics (e_{\min} , Δe , E_c) determined as functions of the number of cycles for the initial state of the alloy and after its surface hardening by EMT and AUFT. We present the data obtained for the last 20000 cycles before fracture: they cover part of the stage with a stable change in the inelasticity characteristics and the stage of accelerated change in the inelasticity parameters. For the EMT-hardened specimens, the range of 20000 cycles includes the entire range of tests (Fig. 4a).

The titanium alloy under study was shown to have low inelasticity parameters (e_{\min} , Δe) at the stage of crack nucleation in all cases of surface hardening during pulsed loading. For example, the hysteresis loop width of the initial alloy at the beginning of tests was 0.0013% and changed weakly up to failure, which is typical of cyclically stable materials at given cycle parameters (Fig. 4b). The average creep rate calculated using the obtained data at the stage of steady creep is 10^{-7} cycle $^{-1}$, which is characteristic of the fatigue fracture of titanium alloys [16].

In all cases, we detected a general character of changing the inelasticity parameters as functions of the number of loading cycles. Specifically, we detected two stages, namely, a steady stage and a stage of an intense change in e_{\min} , Δe , and E_c (see Fig. 4). The first stage is characterized by almost constant values of parameters e_{\min} , Δe , and E_c during cyclic loading. In the second stage, cyclic creep e_{\min} and hysteresis loop width Δe increase intensely and compliance E_c decreases. This behavior is related to the processes of accelerated growth of a main crack and rupture of a specimen [11, 17].

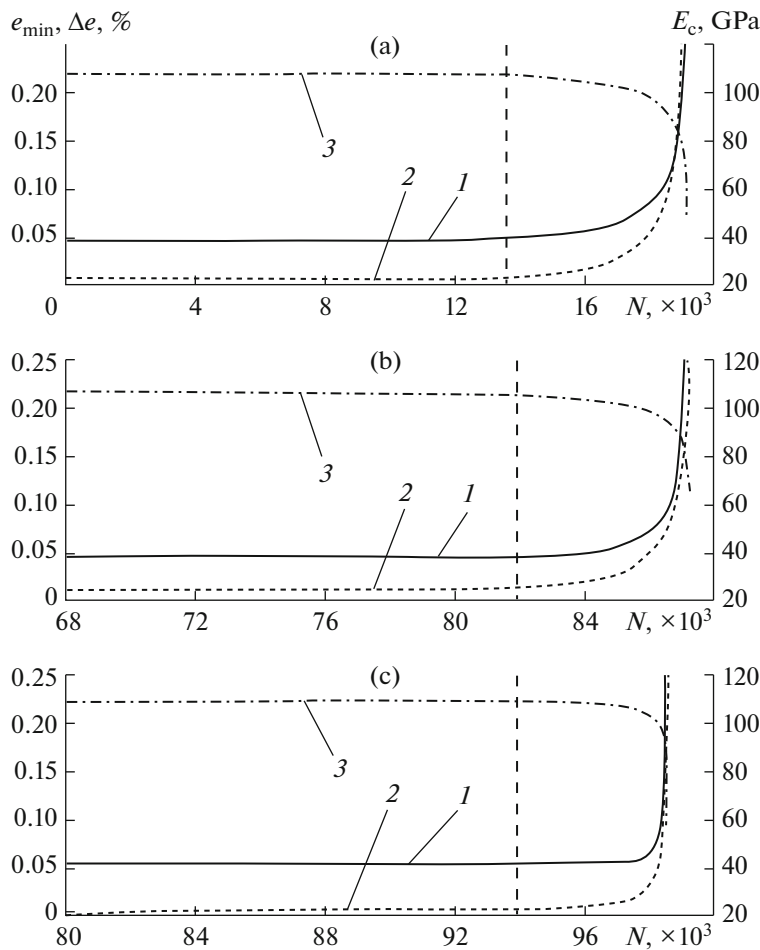


Fig. 4. Change in inelasticity parameters (1) e_{\min} , (2) Δe , and (3) E_c in the last 20000 cycles before fracture for specimens with the following states of surface layer: (a) after EMT, (b) after polishing (initial state), and (c) after AUFT.

For the EMT-hardened specimens, the beginning of the stage of intense changes in the inelasticity parameters corresponds to 13000 cycles (Fig. 4a), and its duration to final fracture is $19100 - 13000 = 6100$ cycles. For specimens in the initial state, this stage begins at 82000 cycles and lasts to fracture of a specimen in 5000 cycles (Fig. 4b). The AUFT-hardened specimens have similar stages of rapid changes in the inelasticity parameters, namely, $98000 - 94000 = 4000$ cycles (Fig. 4c).

A comparison of the curves shown in Fig. 4 demonstrates synchronous changes in the intensities of e_{\min} , Δe , and E_c at the stage of prefracture. Therefore, we can conclude that the stage of intense changes in the inelasticity parameters is determined by simultaneous development of plastic deformation and accelerated crack growth. The duration of the stage of accelerated crack growth and the rupture of a specimen is 4000–6000 cycles irrespective of the total fatigue life of the specimen and the type of surface

hardening (this range is indicated by vertical dashed lines in Fig. 4). A longer fatigue life of a specimen does not affect the stage of accelerated crack growth and rupture.

Stage of Stable Crack Growth

Microfractography, fatigue crack growth parameters. The stage of stable fatigue crack growth during cyclic loading can be characterized by the dependence of the crack growth rate on the stress intensity factor (SIF), which is based on the Paris equation

$$\frac{dl}{dN} = CK_{\max}^n, \quad (1)$$

where dl/dN is the crack growth rate, K_{\max} is the maximum SIF in a cycle, and C and n are the experimental characteristics of the fracture toughness of the material.

The primary reconstruction of the stable crack growth kinetics is performed using fractography based

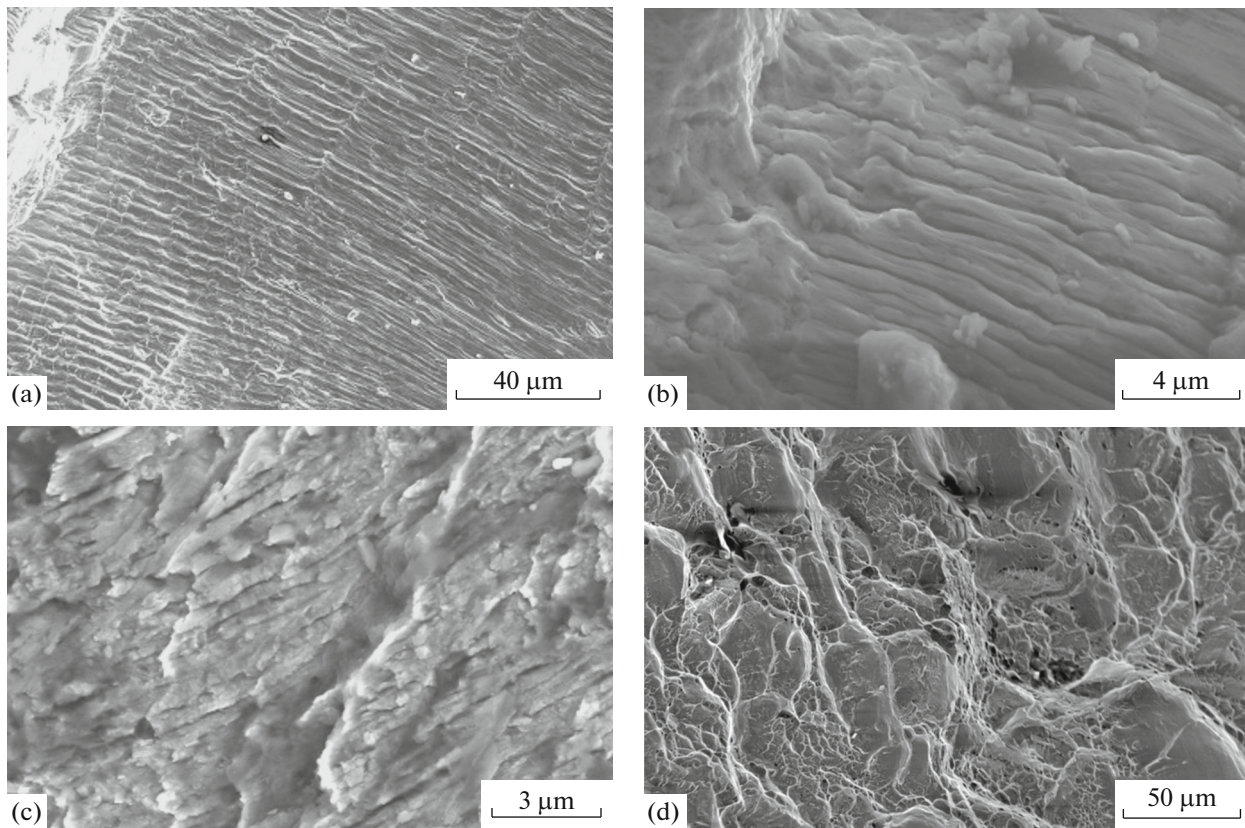


Fig. 5. Micrograph of the fatigue fracture surface in (a–c) stable crack growth zone at various depths ((a) 3.2, (b) 1.5, (c) 1.08 mm) and (d) rupture zone.

on an electron-microscopic analysis of fracture surfaces (Fig. 5). A fracture surface is used to reveal predominant fracture mechanisms at various stages and in various surface zones, from a crack nucleation site to the fracture zone, where a crack reaches critical sizes.

One of the microfractographic signs of stable crack growth is the presence of fatigue grooves on a fracture surface [8, 18, 19]. Distance s between neighboring grooves is determined by the crack growth rate, $s = dl/dN$. The fatigue step, the elastic properties, and SIF K_{\max} at the stage of stable crack growth are related as $s \sim (K_{\max})^n$ [18, 19].

Figures 5a–5c show the fracture surface of the EMT-hardened specimen in the zone of stable crack growth with fatigue grooves, the average distances between at various distances from the crack nucleation site are given in Table 3.

At the stage of rupture, the fracture surface shown in Fig. 5d corresponds to ductile fracture with a pronounced dimple relief.

To estimate the maximum SIF in a cycle K_{\max} as a function of fatigue groove spacing s , we use the expression [18]

$$s = 10K_{\max}^2/E^2, \quad (2)$$

Table 3. Fracture surface parameters in the zone of stable crack growth and the fatigue crack growth characteristics in a PT3V titanium alloy

Parameter	Distance from crack nucleation site, mm		
	3.2	1.5	1.08
s, m	3×10^{-6}	1.2×10^{-6}	7.5×10^{-7}
$K_{\max} \text{ MPa m}^{1/2}$	60.2	41.2	35.0
C		9×10^{-12}	
n		3.17	

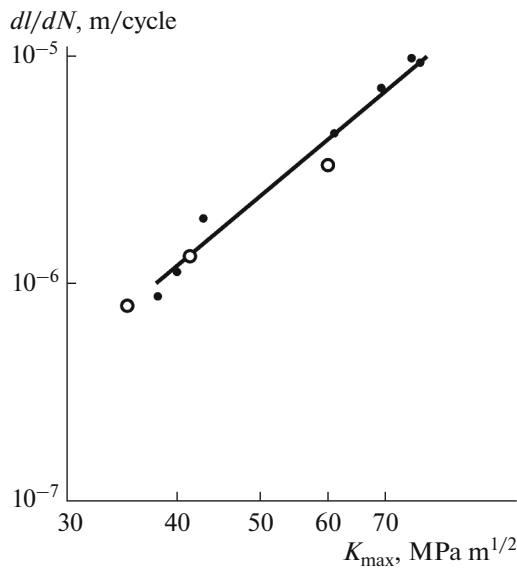


Fig. 6. Fatigue crack growth curve of a PT3V titanium alloy.

where E is the elastic modulus.

Table 3 gives the results of calculating SIF K_{\max} as a function of the groove spacing and the distance from the crack nucleation site. SIF K_{\max} is seen to increase when a crack grows, which is accompanied by an increase in groove spacing s .

To test the reliability of these results, we use the data on the fatigue crack growth in the titanium alloy under study that were obtained from experiments on cyclic three-point bending of prismatic specimens. The diagram plotted using these data is shown as the solid line with solid circles in Fig. 6. The values of SIF K_{\max} calculated by Eq. (2) using the fractographic results are shown as the open circles in Fig. 6. These values are seen to agree well with the experimental results.

Using the microfractographic data (see Table 3), we estimated the duration of the stage of stable crack growth. The number of cycles required for a crack to grow from an initial length to the end of stable growth is determined by integrating Paris equation (1),

$$N = \int_{l_0}^{l_f} \frac{dl}{CK_{\max}^n} = \frac{1}{(2-n)C(F_1\sigma\sqrt{\pi})^n} \times \left(\frac{2-n}{l_f^2} - \frac{2-n}{l_0^2} \right), \quad (3)$$

where l_0 and l_f are the initial and final crack length, respectively, σ is the maximum cycle stress amplitude, and F_1 is a calibration constant [20].

If initial crack length l_0 in Eq. (3) is taken to be comparable with the EMT-hardened layer thickness (0.15 mm), the calculated stage of stable crack growth is 4600 cycles for the limiting value $l_f = 3.2$ mm (see

Table 3). Thus, the durations of the stages of stable and accelerated crack growth and rupture are comparable, about half the fatigue life of the EMT-treated specimens. For specimens of other types, these two stages are $\sim 10\%$ of the total fatigue life.

According to these results, the fracture parameters of the pseudo- α -titanium alloy at the stages of stable fatigue crack growth and rupture weakly depend on the state of the surface layer, including the high-microhardness layer hardened by various methods, at the given level of cyclic stresses. Here, the change in the fatigue life is mainly determined by the stage of crack nucleation, and the role of the state of surface, its mechanical properties, and residual stresses becomes one of the most important factors.

CONCLUSIONS

(1) We studied the influence of various types of hardening of the surface layer in pseudo- α -titanium alloy specimens on the durations of the stages of stable and accelerated crack growth and rupture during pulsed cyclic loading at $\sigma_{\max} = 0.8\sigma_{0.2}$. As follows from the changes in the inelasticity parameters, the hardened surface layer does not affect the stage of accelerated crack growth and rupture during tests of laboratory specimens.

(2) Using the methods of linear fracture mechanics and microfractography, we estimated the duration of the stage of stable crack growth. When laboratory specimens are subjected to fatigue tests, the period of stable crack growth can account for 5–30% of the total fatigue life of the specimens at an insignificant difference between the absolute numbers of cycles.

(3) The key role of the state of surface layer in the total fatigue life of a specimen was supported. The strength estimated from the microhardness was shown not to characterize the ability of material to withstand the nucleation of fatigue cracks.

(4) To achieve a balanced set of the surface microhardness, the strength, the plasticity, and the fatigue life of a PT3V-type titanium alloy, it is reasonable to use a combined surface hardening method with a sequential application of electrochemical and ultrasonic treatment.

FUNDING

This work was supported by the Russian Foundation for Basic Research, project no. 17-08-01742 a.

REFERENCES

1. V. P. Bagmutov, S. N. Parshev, N. G. Dudkina, and I. N. Zakharov, *Electromechanical Treatment: Technological and Physical Principles, Properties, Implementation* (Nauka, Novosibirsk, 2003).
2. V. P. Biryukov, I. M. Petrova, and I. V. Gadolina, "Effect of laser facing on the fatigue resistance charac-

- teristics,” *Mashinost. Inzh. Obraz.*, No. 2, 54–57 (2013).
3. R. R. Valiev, Yu. M. Modina, A. V. Polyakov, I. P. Semenova, and V. S. Zhernakov, “Fatigue strength and fracture of an ultrafine-grained VT6 titanium alloy,” *Vestn. UGATU* **20** (2(72)), 11–16 (2016).
 4. C. Tan, X. Li, Q. Sim, L. Xiao, Y. Zhao, and J. Sun, “Effect of α -phase morphology on low-cycle fatigue behavior of TC21 alloy,” *Int. J. Fatigue*, No. 75, 1–9 (2015).
 5. M. B. Sazonov and L. V. Solovatskaya, “Stresses in the surface layer of a part after hardening by various surface plastic deformation methods,” *Vestn. Samar. Gos. Aerokosmich. Univ.* **14** (3), 467–473 (2015).
 6. X. Yuan, Z. P. Yue, S. F. Wen, L. Li, and T. Feng, “Numerical and experimental investigation of the cold expansion process with split sleeve in titanium alloy TC4,” *Int. J. Fatigue*, No. 77, 78–85 (2015).
 7. T. M. Mower, “Degradation of titanium 6Al–4V fatigue strength due to electrical discharge machining,” *Int. J. Fatigue* (2014).
<https://doi.org/10.1016/j.ijfatigue.2014.02.018>
 8. B. K. Pant, A. H. V. Pavan, R. V. Prakash, and M. Kamaraj, “Effect of laser peening and shot peening on fatigue striations during FCGR study of Ti6Al4V,” *Int. J. Fatigue* (2016).
<https://doi.org/10.1016/j.ijfatigue.2016.08.005>
 9. B. Brenner, Sh. Bonss, F. Titts, I. Kaspar, and D. Val’ter, “Method of producing wear-resistant and high-fatigue-strength surface layers on parts of titanium alloys and the part fabricated by this method,” RF Patent 2407822, 2005.
 10. V. F. Terent’ev and S. A. Korableva, *Fatigue of Metals* (Nauka, Moscow, 2015).
 11. V. T. Troshchenko, “Scattered fatigue damage of metals and alloys. I. Inelasticity, methods, and experimental results,” *Probl. Prochn.*, No. 4, 5–32 (2005).
 12. A. N. Pomanov, “Problems of materials science in the mechanics of deformation and fracture at the stage of crack formation,” *Vestn. Nauch.-Tekh. Razvitiya*, No. 11 (75), 38–49 (2013).
 13. V. P. Bagmutov, V. I. Vodop’yanov, I. N. Zakharov, A. I. Gorunov, and D. S. Denisevich, “Effect of intense thermomechanical treatment on the structure and properties of titanium pseudo- α alloys during electromechanical treatment,” *Russ. Metall. (Metally)*, No. 9, 712–715 (2013).
 14. V. P. Bagmutov, V. I. Vodop’yanov, I. N. Zakharov, and D. S. Denisevich, “Relation between the fracture laws and the fatigue life of a surface-hardened pseudo- α -titanium alloy,” *Russ. Metall. (Metally)*, No. 7, 663–668 (2016).
 15. V. P. Bagmutov, D. S. Denisevich, I. N. Zakharov, and A. Yu. Ivannikov, “Taking into account the nonlinear and coupled effects of the thermal problem and phase transitions during the simulation of contact thermomechanical surface hardening of metallic alloys,” *PNRPU Mechan. Bull.*, No. 1, 233–250 (2017).
 16. I. V. Gorynin and B. B. Chechulin, *Titanium in Machine Building* (Mashinostroenie, Moscow, 1990).
 17. V. F. Terent’ev, “Cyclic strength of submicro- and nanocrystalline metals and alloys (review),” *Novye Mater. Tekhnol. Metallurg. Mashinost.*, No. 1, 8–24 (2010).
 18. N. V. Tumanov et al., “Simulation of the stable fatigue crack growth in the turbine disks in an aircraft engine in simple and complex loading cycles,” *Vestn. Samar. Gos. Aerokosmich. Univ.*, No. 3 (19), 188–199 (2009).
 19. A. A. Shanyavskii, *Safe Fatigue Fracture of Aviation Construction Elements. Synergy in Engineering Applications* (Monografiya, Ufa, 2003).
 20. *Handbook of the Stress Intensity Factors*, Ed. by Yu. Murakami (Mir, Moscow, 1990), Vol. 2.

Translated by K. Shakhlevich